Magnetic Resonance in Medicine 65:1570–1577 (2011)

Real-Time Functional MRI Using Pseudo-Continuous Arterial Spin Labeling

Luis Hernandez-Garcia,[1,2]* Hesamoddin Jahanian,[2] Mark K. Greenwald,[3] Jon-Kar Zubieta,[4] and Scott J. Peltier[1,2]

The first implementation of real-time acquisition and analysis of arterial spin labeling-based functional magnetic resonance imaging time series is presented in this article. The implementation uses a pseudo-continuous labeling scheme followed by a spiral *k*-space acquisition trajectory. Real-time reconstruction of the images, preprocessing, and regression analysis of the functional magnetic resonance imaging data were implemented on a laptop computer interfaced with the MRI scanner. The method allows the user to track the current raw data, subtraction images, and the cumulative *t*-statistic map overlaid on a cumulative subtraction image. The user is also able to track the time course of individual time courses and interactively selects a region of interest as a nuisance covariate. The pulse sequence allows the user to adjust acquisition and labeling parameters while observing their effect on the image within two successive pulse repetition times. This method is demonstrated by two functional imaging experiments: a simultaneous finger-tapping and visual stimulation paradigm, and a bimanual finger-tapping task. Magn Reson Med 65:1570–1577, 2011. © 2011 Wiley-Liss, Inc.

Key words: arterial spin labeling; real time; fMRI

Conventional functional magnetic resonance imaging (fMRI) collects blood oxygen level-dependent (BOLD)-contrast MR images of a subject's brain while performing a cognitive task, whereas subsequent image reconstruction and analysis are performed offline (i.e., on a separate computer after the experiment is completed). Real-time fMRI is an exciting extension to conventional fMRI techniques that enables the user to analyze fMRI data as it is being collected. Thus, in real-time fMRI, the results are immediately available as the subject is being scanned, and the results can be used to reveal and guide the subject's cognitive processes. It can also facilitate the experimenter's parameter selections or a clinician's interventions (1).

Several real-time analysis methods have been implemented for online processing of BOLD data, including cumulative correlation (2), sliding-window correlations with reference vector optimization (3), online general linear model analysis (4), and combined methods to collect behavioral, physiological, and MRI data while performing near real-time statistical analysis (5). All the above methods can facilitate real-time analysis, e.g., the incremental algorithms are useful in monitoring ongoing activation, and the sliding window approaches can improve localization of dynamic activity in time (4). Given current computer-processing speed, any of these approaches can be used to display real-time activation maps. This allows for several real-time applications: online data quality control, real-time functional activation monitoring, interactive paradigms based on the subject's dynamic functional activity (fMRI biofeedback or brain-computer interface; Ref. 6), and autonomous control of neural activation using real-time fMRI. These techniques have been used to study subjects' modulation of motor-area cortical activation and emotional processing (7–11).

However, despite the efficiency of BOLD-contrast MR images to detect and localize active site in fMRI, the BOLD signal is difficult to quantify in a physically meaningful way because it results from intricate relationships between cerebral oxygenation, blood flow and volume, as well as the scanner's unique characteristics. Because of very limited processing time available in real-time fMRI applications, quantifying the BOLD signal in real time poses substantial challenges. Furthermore, the baseline of the BOLD signal drifts over time within a session, and this could be quite problematic in experiments where the periodicity of the paradigm is quite long. The lack of meaningful physical units in BOLD data, in addition to these drifts, challenges the use of BOLD imaging for studies of baseline activity and confound long-term activation studies considerably (12).

Given the quantitative nature of its signal and its insensitivity to signal drifts of the scanner, perfusion-based fMRI using arterial spin labeling (ASL) techniques have emerged as an alternative to BOLD fMRI. ASL techniques (13–15) use magnetically labeled arterial water as an endogenous tracer to quantify the perfusion rate. This type of measurement is particularly desirable for longitudinal studies and studies with low stimulation frequency, where the BOLD signal drifts are confounded with the signal of interest (16–18). Because of inherently low signal-to-noise ratio (SNR) and contrast-to-noise ratio (CNR) in ASL techniques, the use of ASL-based fMRI is more challenging than BOLD-based fMRI. SNR maps for BOLD data reported in Ref. 19 have values about 50 times higher than those of ASL. Yang et al. (20) also reported *t*-

[1]Functional MRI Laboratory, University of Michigan, Ann Arbor, Michigan, USA.
[2]Department of Biomedical Engineering, University of Michigan, Ann Arbor, Michigan, USA.
[3]Department of Psychiatry and Neuroscience, Wayne State University School of Medicine, Detroit, Michigan, USA.
[4]Department of Psychiatry, University of Michigan, Ann Arbor, Michigan, USA.
Grant sponsor: NIH; Grant numbers: EB004346, DA026077.
*Correspondence to: Luis Hernandez-Garcia, PhD, Functional MRI Laboratory, University of Michigan, 2360 Bonisteel Blvd., Ann Arbor, MI 48105.
E-mail: hernan@umich.edu
Received 19 November 2010; revised 22 February 2011; accepted 23 February 2011.
DOI 10.1002/mrm.22922
Published online 28 March 2011 in Wiley Online Library (wileyonlinelibrary.com).

scores of ~5 for ASL data versus *t*-scores greater than 10 for BOLD data. Therefore, the SNR of ASL experiments can be boosted by increasing the length of the stimulation blocks if the cognitive paradigm permits it, as explored at length by Aguirre et al. (21). At the same time, real-time imaging with ASL is facilitated by the fact that there is a long period of labeling between image acquisitions.

We note that, in the realm of clinical perfusion imaging with ASL, Xie et al. (22) have developed an adaptive sampling scheme that can determine an optimal set of inversion times for baseline perfusion quantification with pulsed ASL images. This method examines the images collected and determines the choice of inversion time for the next image within the acquisition period, i.e., in real time; however, it must be noted that this technique is not related to time series fMRI.

In this article, we introduce the first implementation, to our knowledge, of real-time ASL-based fMRI. The aims of this communication are to report on the technical feasibility of acquiring perfusion-based functional images using ASL in real time and on the necessary software interfaces and analysis methods for image acquisition and process. Our implementation uses a pseudo-continuous labeling scheme (23) followed by a spiral *k*-space acquisition trajectory. It allows interactive adjustment of parameters, data smoothing, differencing, statistical analysis, and display during acquisition of individual ASL images. It also enables the user to track the time course of individual voxels and to select a region of interest (ROI) as a nuisance covariate interactively. The interface is implemented on a laptop computer interfaced with the MRI scanner.

We demonstrate our implementation of real-time ASL on a simple visual-motor activation experiment and on a bimanual finger opposition task, although the long-term application motivating this work is fMRI-guided biofeedback to train nicotine-dependent subjects to control their cigarette craving.

MATERIALS AND METHODS

This work was performed on a 3.0-T GE Signa scanner (Waukesha, WI) interfaced with an Apple MacBook Pro (Cupertino, CA) with a 2.4-GHz dual-core processor and 4 GB of RAM. The acquisition pulse sequence was a pCASL sequence (23) with (a) phase corrections (26,27) for optimization of labeling efficiency, (b) real-time communication support, and (c) spiral trajectory image acquisition (field of view = 24 cm, slice thickness = 6 mm, data matrix = 64 × 64 × 8 slices). Each slice generated 4712 complex data points of raw *k*-space data. The pCASL pulse train had the following parameters: pulse repetition time (TR) = 4000 ms, tagging time = 2100 ms, postinversion delay = 1500 ms, pCASL flip angle = 35°, fractional moment = 0.9, pCASL TR = 1.5 ms, pCASL phase correction = 2.2 radians.

A diagram of the data flow is shown in Fig. 1. Data transfer between the scanner and the MacBook was done through Ethernet using custom C functions modified from the RDS Client software (General Electric Medical Systems, Waukesha, WI). Data were transferred directly from the scanner's data acquisition board to the laptop's memory via TCP/IP connection, without disk storage. Reconstruction, processing, and display were performed off-line by the MacBook using custom Matlab Software (South Nattick, MA). Transfer and reconstruction were performed after each slice acquisition. To reduce memory requirements, the reconstructed images were analyzed as single-precision floating-point numbers instead of Matlab's default double precision. Data were smoothed with a gaussian kernel, and running subtraction was performed on the images to yield perfusion-weighted images. A reference function reflecting the effects of interest (i.e., the perfusion response to the stimulation paradigm) was constructed prior to the experiment. The reference function consisted of a box-car function convolved with a gamma-variate hemodynamic impulse response function. This function was used to create a design matrix for general linear model analysis that also included a nuisance regressor, which was updated during the data acquisition, and a baseline regressor. As the *n*th image was acquired, a temporary design matrix was updated from the first *n* rows of the whole design matrix. The parameters of this temporary general linear model were estimated by ordinary least squares, and a *t*-statistic map was computed for the contrast of interest. *T*-maps were overlaid on the mean perfusion-weighted image and thresholded at a liberal $|t| > 3.0$. The aforementioned nuisance regressor consisted of the time course at an ROI selected by the user in real time. This ROI was chosen from a white matter region to remove physiological fluctuations or other spatial correlations in ASL data. All calculations, including image reconstruction, were executed within a single TR (4 s).

The global mean time course, the reference function, and the time courses of the user-defined "nuisance region" and a second ROI were displayed in real time. This allowed the user to monitor activation in any specific brain area and to inspect the nuisance regressor for correlations with the reference function visually. The user was thus able to choose both ROIs in real time.

For testing and demonstration purposes, two subjects were scanned in accordance with the University of Michigan's Internal Review Board's policies. A real-time pCASL time series was collected while the first subject performed a finger-tapping task consisting of 20-s tapping with the left hand while a checkerboard pattern flashed in front of the subject's eyes at 8 Hz. The activation period was followed by 30 s rest. This 50-s cycle was repeated over a 320-s period. The second subject was instructed to perform a finger-tapping task with the right hand for 20 s, followed by 20-s finger tapping with the left hand. This procedure was repeated for 320 s. In both cases, the data were transferred, reconstructed, and processed, as described above, while the user updated the nuisance ROI and monitored the image acquisition quality and statistical map in real time.

RESULTS

After every acquisition, the following displays were updated: (1) current reconstructed image, (2) the most

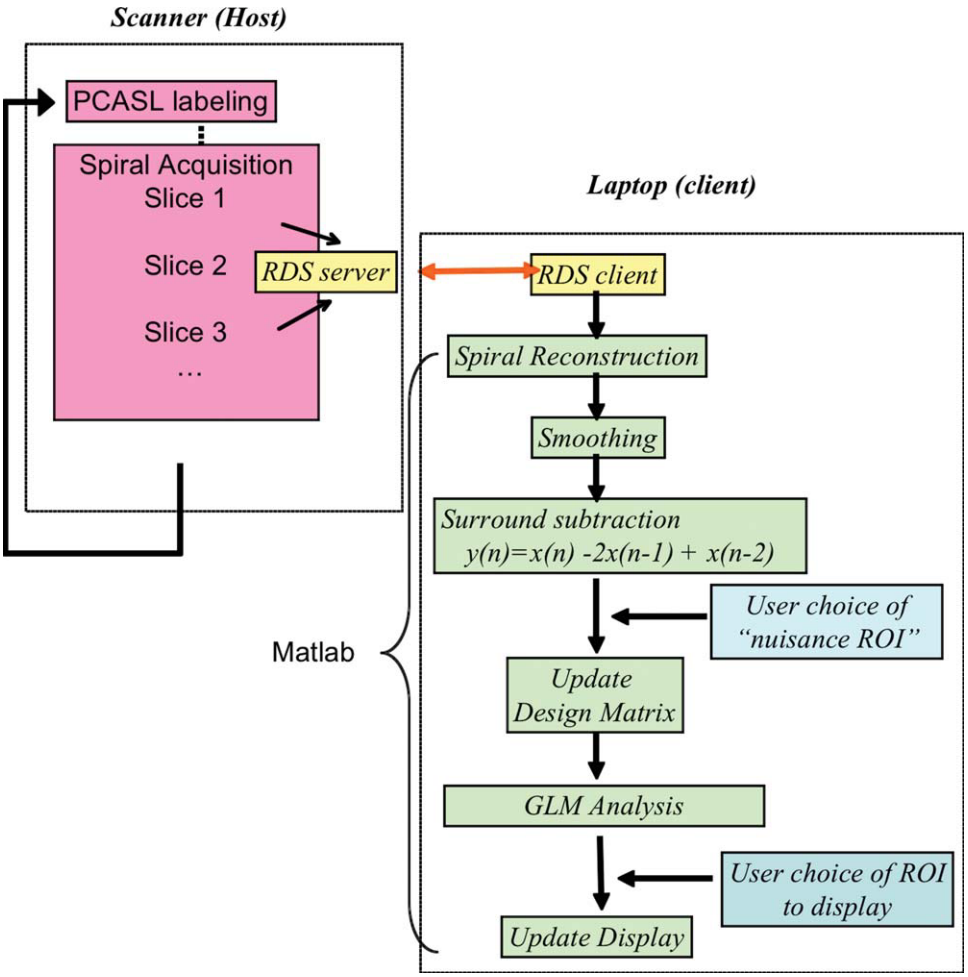

FIG. 1. Real-time processing stream for ASL fMRI experiment. Data were transferred directly from the scanner's data acquisition board to laptop memory without disk storage. Reconstruction, processing, and display were performed online by the MacBook using custom Matlab software. Transfer and reconstruction were performed after each slice acquisition. The user interacts with the system by selecting the ROI for the nuisance regressor and a second ROI for time series display.

recent perfusion-weighted image, (3) the thresholded *t*-statistic map overlaid on the mean perfusion-weighted image, and (4) a time course of the spatial mean ASL signal over the field of view, a user-selected ROI, and a second ROI that serves as a nuisance regressor. The model waveform was also displayed for reference. The Matlab reconstruction, processing, and display program was able to keep in real time (processing lag < 2 TR) with the acquisition. Each slice reconstruction from the spiral *k*-space data took 0.02 s on average. The computation time of the ordinary least squares over the whole volume increased linearly with the number of time points available, from 0.38 s at the third acquisition up to 0.57 s at the 80th acquisition.

For each subject, a sample screenshot of the user interface taken after 80 acquisitions is displayed in Figs. 2 and 3. Positive *t*-scores are displayed in a red color scale, whereas negative *t*-scores are displayed on a blue color scale. As expected, the visual-motor task (subject 1) produced increases in perfusion that correlated with the reference function in the right motor cortex and the visual cortex. The bimanual motor task (subject 2) resulted in perfusion increases that were correlated with the reference function on the left motor cortex and anticorrelated on the right motor cortex. Figure 4 shows the evolution of the *t*-statistic map throughout the acquisition for the first subject.

We note that, as a result of spiral acquisition without fat saturation pulses, a circular rim appears around the brain in the raw images shown in Figs. 2 and 3. This is the off-resonance signal arising from fat saturation pulses and it disappears on subtraction of the control and tagged images, as indicated in the second and third panels.

The effectiveness of removing unwanted variance changes depending on the user's choice of ROI. Thus, we explored four ROIs (post hoc) as sources of a nuisance regressor and compared the results in terms of their effect on the *t*-statistic maps. The four ROIs consisted of the posterior cerebral artery (PCA), the anterior cerebral artery (ACA), a white matter (WM) region, and a heavily vascularized area in the left insula (Ins). These ROIs are indicated in Fig. 2. Figure 5 shows maps of the decrease in residual variance maps due to inclusion of each nuisance regressor in the design matrix. This figure indicates that by selecting ROIs in the PCA, the residual variance was reduced most dramatically in the vascular tree. Interestingly, selecting the ACA also reduced the residual variance on a wide region along the frontal edge of the brain. Indeed, high variance along the rim of the brain in fMRI studies is usually indicative of bulk head movement (personal observation). Because the ACA ROI was next to the brain's edge, it is likely that this time course contained a large amount of partial

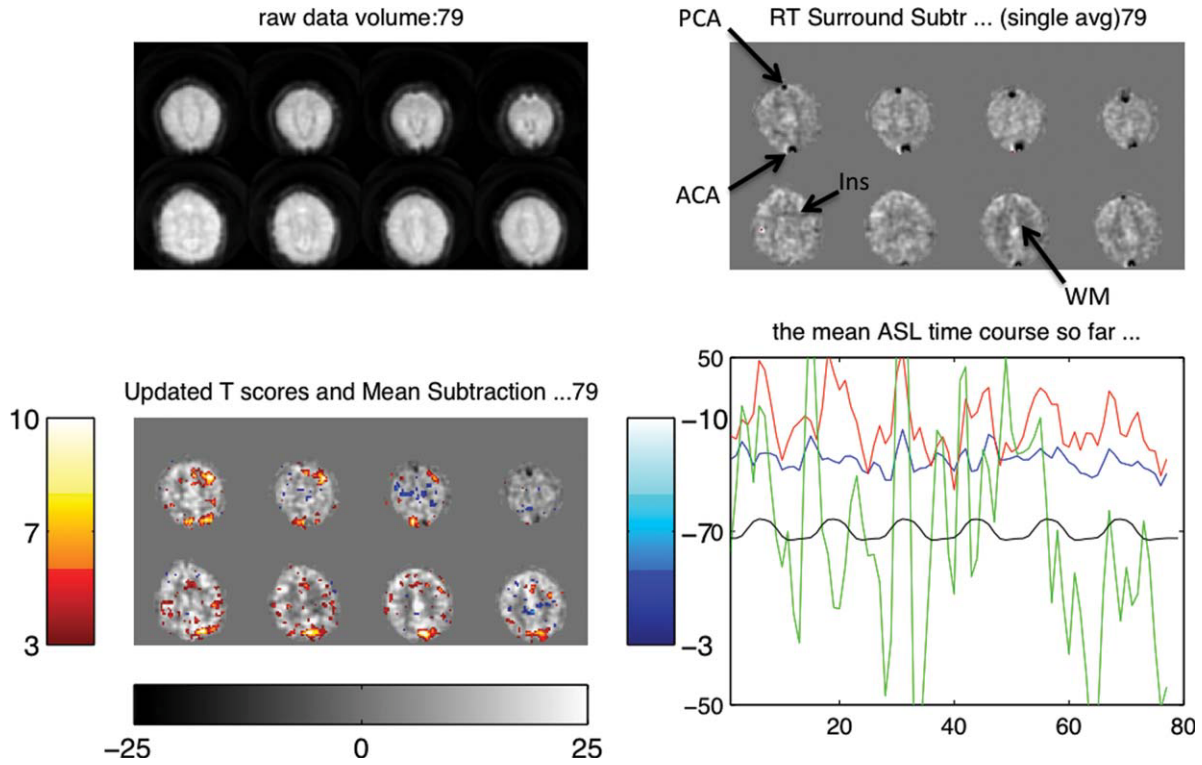

FIG. 2. User interface of real-time system: visual-motor task. Screenshot of the user interface during real-time acquisition. Clockwise, the panels display the most current unsubtracted image, the most current subtracted image, a plot of relevant time courses, and the most current update of the statistical map overlaid on the mean of the perfusion weighted images. The time courses plotted on the lower right are the reference model function in black; the nuisance time course in green; the spatial mean of the ASL image time course in blue; and the time course of a pixel of interest after nuisance removal in red. Four ROIs used as nuisance covariates are indicated in the top-right panel. These ROIs consisted of a 3 × 3 voxel region sampled at a single slice. The regions were placed on the posterior cerebral artery (PCA), the anterior cerebral artery (ACA), a white mater region (WM), and a heavily vascularized left insula region (Ins).

volume changes arising from the subject's movement. The WM ROI caused a modest and fairly uniform reduction in residual variance (note the difference in color scales). The left insular region's effect was also modest, relative to PCA and ACA, but was most noticeable in vascular regions, like the PCA and ACA.

The effect of nuisance covariates on the *t*-score distribution can be seen in Fig. 6. Not surprisingly, the largest effect was obtained when vascular regions were used as the source of the nuisance covariate. Selecting either the ACA or the PCA as nuisance sources reduced the width of the *t*-score distribution and shifted its peak toward zero. However, the distribution in larger *t*-score range remained largely unchanged, suggesting a boost in specificity (reduced the number of false positives), while sensitivity remained largely unchanged (the number of true positives detected remained). The number of activated voxels ($T > 3$) obtained using ACA, WM, Ins, and PCA for nuisance covariates are 1091, 1174, 1174, and 924, whereas they were 1173 without use of the nuisance covariate.

The spatial distribution of these differences in the *t*-score maps due to the nuisance regressors can be seen in Fig. 7. We noted that the effects of the WM and insula regressors were subtler than the arterial ROIs. The WM ROI, however, boosted *t*-scores largely in the visual and right-motor cortices and not in other regions. Inclusion of the PCA regressor reduced the *t*-scores in arterial regions and boosted the *t* scores in the visual cortex, but appeared to have little effect in the motor cortex.

DISCUSSION

In this communication, we have demonstrated that real-time ASL fMRI reconstruction, display, and analysis can be performed on a personal computer. Our target application is to provide neuroimaging feedback to experimental subjects undergoing stimulation paradigms with very long periodicity (>45 s). Therefore, real-time ASL scanning can be quite useful in the fMRI setting for many applications, in addition to our own application. Primarily, it allows the operator to evaluate data quality immediately. This point is important because ASL data have an inherently low signal-to-noise ratio, exacerbated by low inversion efficiency, which can be a problem in certain ASL implementations such as amplitude modulated control (24). In addition, field inhomogeneities can compromise the inversion efficiency of some ASL techniques such as pCASL (25–27). Hence, we find it extremely useful to be able to evaluate data quality and make decisions about tuning the labeling parameters immediately. The technique also affords the user the opportunity to quickly evaluate the subject's performance during the scanning session itself. Furthermore, it allows the investigator to determine the subject's

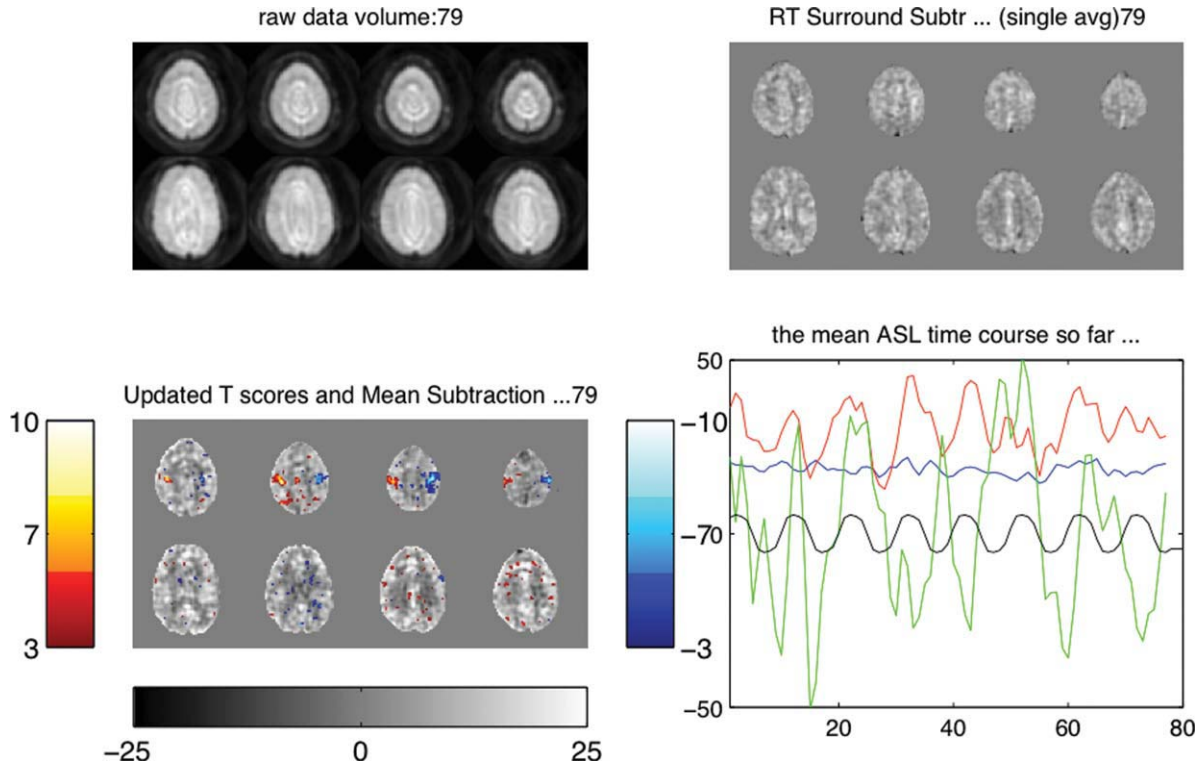

FIG. 3. User interface of real-time system: alternating finger-tapping task. As in Fig. 2, the raw image, subtracted images, statistical maps, and time courses are displayed in real time. In this case, the activation maps indicated correlation with the reference function in the left motor cortex and anticorrelation on the right motor cortex, corresponding to the alternating finger-tapping task.

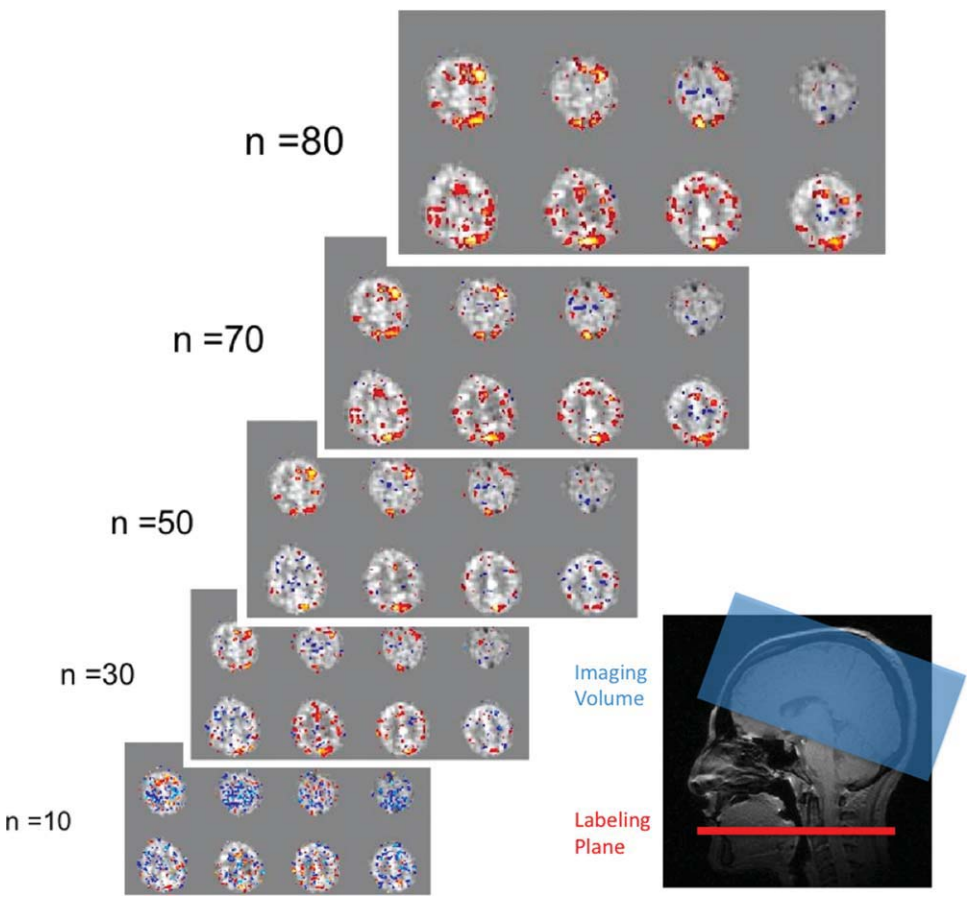

FIG. 4. Evolution of the statistical map during visual-motor stimulation task. As more data were available, the statistical maps became more detailed with a lower number of false positives and more significant scores in the active regions. The placement of the inversion plane and the imaging slices relative to each other is shown on a sagittal view.

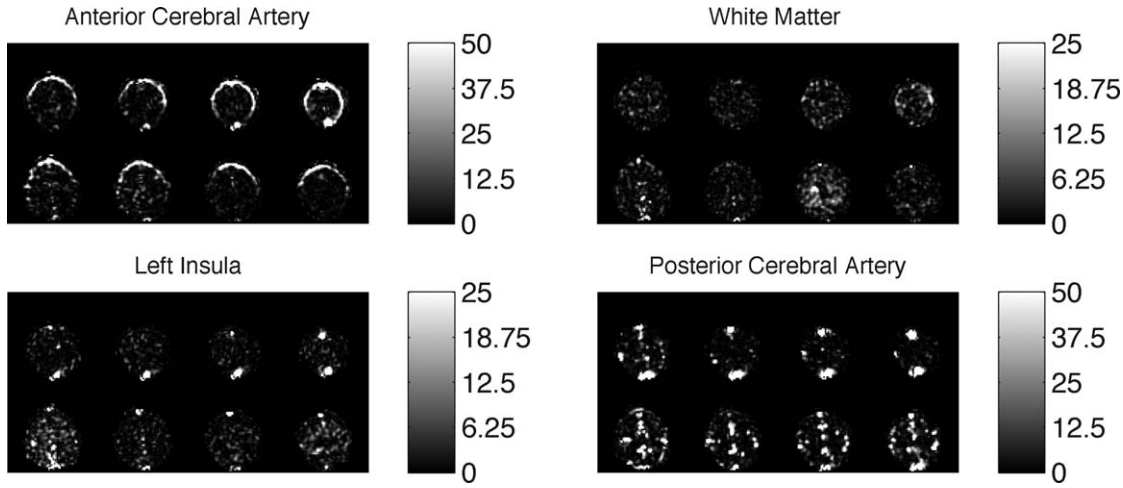

FIG. 5. Effects of nuisance regressor on residual variance map. The maps display the change in the residual variance caused by including the nuisance regressor in the design matrix. The greatest variance reduction was observed when choosing nuisance ROIs in the vasculature.

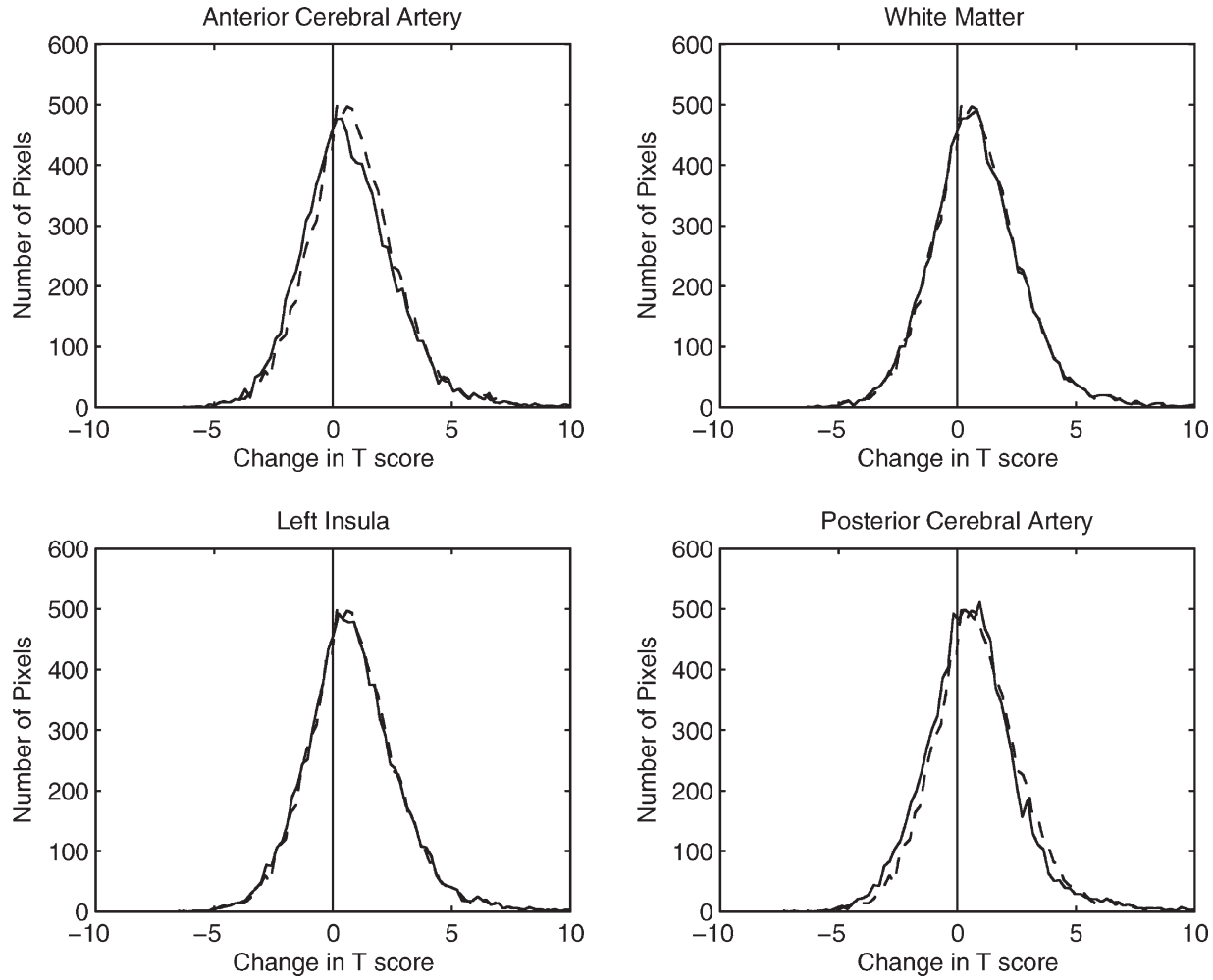

FIG. 6. Effects of nuisance regressor on the statistical map's distribution. The distributions of the changes in *t*-scores over the image produced by the inclusion of nuisance regressors (see Fig. 5) are displayed as histograms. The broken line corresponds to the *t*-distribution obtained without the nuisance regressor, whereas the solid line corresponds to the distribution after including the nuisance regressor. Nuisance regressors obtained from the anterior and posterior cerebral arteries produced a shift of the peak toward zero and a reduction of the distribution's width. We also note that the *t*-score distribution in the larger regions was largely unchanged.

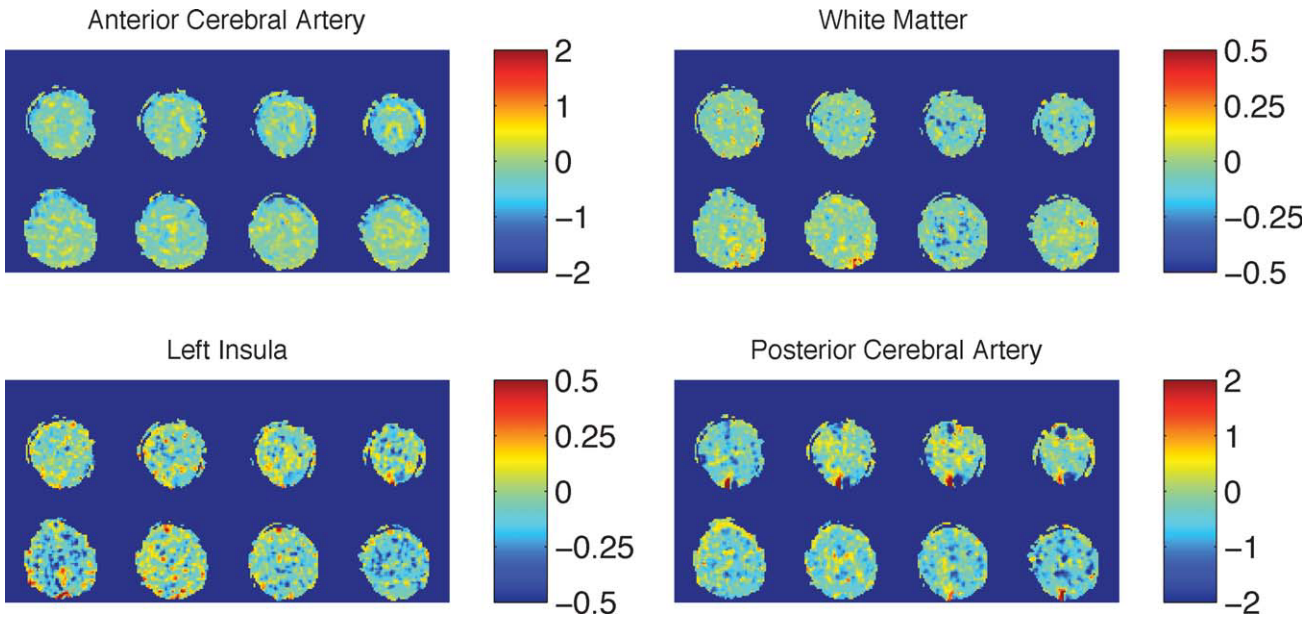

FIG. 7. Effects of Nuisance regressor on statistical map. The change in the *t*-maps produced by the inclusion of nuisance regressors can be seen on this figure. The effect of the white matter and insula regressors was subtler (note the color scales) than the arterial ROIs. The white matter ROI, however, boosted *t*-scores largely in the visual and right-motor cortices. Inclusion of the PCA regressor reduced *t*-scores in arterial regions and boosted *t*-scores in the visual cortex, but appeared to have little effect in the motor cortex.

compliance with the task and/or to make decisions about subsequent stimuli or interactions with the subject.

Real-time imaging with ASL is facilitated by the fact that there is a long period of labeling between image acquisitions. This labeling period affords the user with ample time for reconstruction, image corrections, and analysis "on the fly." We are presently developing more sophisticated methods to analyze the data, including pattern recognition methods based on support vector machine classification (28). In our current implementation, the 4-s TR offered ample time to process the data using linear regression, even as the size of the data and design matrices increased. For longer time series or reduced TR times, such as those using Turbo-CASL techniques (29,30), sliding window or incremental regression techniques (4,31) may be necessary.

As with other ASL fMRI acquisitions, the number of slices that can be acquired is restricted by system acquisition speed. The kinetics of the inversion label are such that the entire volume should be collected within an approximately 500 ms window to ensure that the label has sufficient time to arrive at the tissue but not enough to have washed out completely. Although our acquisition scheme used a sequential slice acquisition, 3D imaging schemes for data acquisition may also prove to be beneficial, as demonstrated in Ref. 33. Parallel imaging will also increase acquisition speed, although at a penalty of computation time (19), and therefore, it may require a faster computing framework. Parallel computing technology and graphics processing units can be used to achieve the necessary computational speed for reconstruction and processing (32).

The use of the ROI's time course as a nuisance covariate improved the analyses. An in-depth study of noise removal by nuisance ROI covariates is outside the scope of this article; however, we note that Wang et al. (34) demonstrated that using the global mean signal as a covariate modestly improved sensitivity by removing spatially coherent noise from the time series, provided that the global signal was not correlated with the reference function. Behzadi et al. (35) also noted that using time courses from pixels with high variance to construct nuisance covariates had a significant effect for noise removal and that these high-variance ROIs corresponded largely with the arterial vasculature. Arterial fluctuations are quite visible to the naked eye in ASL time series data, especially when displayed as a movie. As ASL data are collected and displayed in real time, the signal intensity in arteries fluctuates with the cardiac cycle, and the subtraction process enhances this fluctuation making the arteries quite evident to the user. These fluctuations are also pervasive on the rest of the image, although to a less dramatic extent, and therefore, it is not surprising that including their time course as a nuisance regressor was beneficial for the analysis. Thus, real-time acquisition and processing greatly facilitated the choice of a nuisance regressor. The user can thus pick one such region as a nuisance covariate and immediately observe its effect on the time course of the ROI as well as on the *t*-map obtained from the general linear model estimation. However, this approach must be used with care and with some prior knowledge of the expected activation pattern and brain vasculature. In general, standard angiographic techniques are not necessary to identify major arteries, as the oscillations in the ASL signal make them quite apparent to the user. It is important, however, that the user does not select a nuisance region whose activity is task related, as that can result in a loss of sensitivity

and detection power. Hence, it is useful to display the reference time course along with the nuisance regressor to identify potential correlations. We also note that including additional nuisance regressors always results in loss of degrees of freedom and, while reducing the residual variance and boosting the *t*-statistics, they can potentially reduce the statistical significance of the result.

CONCLUSION

In conclusion, we have demonstrated the first implementation of real-time acquisition and analysis of ASL-based fMRI time series. All calculations, including image reconstruction, were executed within a single TR (4 s). Our pulse sequence allows the user to adjust acquisition and labeling parameters while observing their effect on the image within two successive TRs. We were able to achieve the reconstruction and analysis on a laptop computer interfaced with the MRI scanner. By tracking individual time courses and by interactively selecting an ROI as a nuisance covariate, we were able to improve signal detection in real time.

REFERENCES

1. deCharms RC. Applications of real-time fMRI. Nat Rev Neurosci 2008;9:720–729.
2. Cox RW, Jesmanowicz A, Hyde JS. Real-time functional magnetic resonance imaging. Magn Reson Med 1995;33:230–236.
3. Gembris D, Taylor JG, Schor S, Frings W, Suter D, Posse S. Functional magnetic resonance imaging in real time (FIRE): sliding-window correlation analysis and reference-vector optimization. Magn Reson Med 2000;43:259–268.
4. Nakai T, Bagarinao E, Matsuo K, Ohgami Y, Kato C. Dynamic monitoring of brain activation under visual stimulation using fMRI—the advantage of real-time fMRI with sliding window GLM analysis. J Neurosci Methods 2006;157:158–167.
5. Voyvodic JT. Real-time fMRI paradigm control, physiology, and behavior combined with near real-time statistical analysis. Neuroimage 1999;10:91–106.
6. Yoo SS, Fairneny T, Chen NK, Choo SE, Panych LP, Park HW, Lee SY, Jolesz FA. Brain-computer interface using fMRI: spatial navigation by thoughts. Neuroreport 2004;15:1591–1595.
7. Yoo SS, Jolesz FA. Functional MRI for neurofeedback: feasibility study on a hand motor task. Neuroreport 2002;13:1377–1381.
8. Posse S, Fitzgerald D, Gao KX, Habel U, Rosenberg D, Moore GJ, Schneider F. Real-time fMRI of temporolimbic regions detects amygdala activation during single-trial self-induced sadness. Neuroimage 2003;18:760–768.
9. deCharms RC, Christoff K, Glover GH, Pauly JM, Whitfield S, Gabrieli JDE. Learned regulation of spatially localized brain activation using real-time fMRI. Neuroimage 2004;21:436–443.
10. Phan KL, Fitzgerald DA, Gao K, Moore GJ, Tancer ME, Posse S. Real-time fMRI of cortico-limbic brain activity during emotional processing. Neuroreport 2004;15:527–532.
11. Caria A, Veit R, Sitaram R, Lotze M, Weiskopf N, Grodd W, Birbaumer N. Regulation of anterior insular cortex activity using real-time fMRI. Neuroimage 2007;35:1238–1246.
12. Boynton G, Engel S, Glover G, Heeger D. Linear systems analysis of functional magnetic resonance imaging in human V1. J Neurosci 1996; 16:4207–4221.
13. Alsop D, Detre J. Reduced transit-time sensitivity in noninvasive magnetic resonance imaging of human cerebral blood flow. J Cereb Blood Flow Metab 1996;16:1236–1249.
14. Detre J, Leigh J, Williams D, Koretsky A. Perfusion imaging. Magn Reson Med 1992;23:37–45.
15. Williams D, Detre J, Leigh J, Koretsky A. Magnetic resonance imaging of perfusion using spin inversion of arterial water. Proc Natl Acad Sci USA 1992;89:212–216.
16. Aguirre G, Detre J, Zarahn E, Alsop D. Experimental design and the relative sensitivity of BOLD and perfusion fMRI. Neuroimage 2002; 15:488–500.
17. Liu T, Wong E. A signal processing model for arterial spin labeling functional MRI. Neuroimage 2005;24:207–215.
18. Liu T, Wong E, Frank L, Buxton R. Analysis and design of perfusion-based event-related fMRI experiments. Neuroimage 2002;16:269–282.
19. Perthen JE, Bydder M, Restom K, Liu TT. SNR and functional sensitivity of BOLD and perfusion-based fMRI using arterial spin labeling with spiral SENSE at 3 T. Magn Reson Imaging 2008;26:513–522.
20. Yang Y, Gu H, Stein AE. Simultaneous MRI acquisition of blood volume, blood flow, and blood oxygenation information during brain activation. Magn Reson Med 2004;52:1407–1417.
21. Aguirre GK, Zarahn E, D'Esposito M. The variability of human, BOLD hemodynamic responses. Neuroimage 1998;8:360–369.
22. Xie J, Clare S, Gallichan D, Gunn RN, Jezzard P. Real-time adaptive sequential design for optimal acquisition of arterial spin labeling MRI data. Magn Reson Med 2010;64:203–210.
23. Dai W, Garcia D, de Bazelaire C, Alsop DC. Continuous flow-driven inversion for arterial spin labeling using pulsed radio frequency and gradient fields. Magn Reson Med 2008;60:1488–1497.
24. Wang J, Zhang Y, Wolf R, Roc A, Alsop D, Detre J. Amplitude-modulated continuous arterial spin-labeling 3.0-T perfusion MR imaging with a single coil: feasibility study. Radiology 2005;235:218–228.
25. Jung Y, Wong EC, Liu TT. Multiphase pseudocontinuous arterial spin labeling (MP-PCASL) for robust quantification of cerebral blood flow. Magn Reson Med 2010;64:799–810.
26. Jahanian H, Hernandez-Garcia L, Noll DC. Correcting for off-resonance induced degradation of inversion efficiency in pseudo-continuous ASL. In: Proceedings of the 17th Annual Meeting of the ISMRM, Honolulu, Hawaii; 2009. p 1518.
27. Jahanian H, Noll D, Hernandez-Garcia L. B(0) field inhomogeneity considerations in pseudo-continuous arterial spin labeling (pCASL): effects on tagging efficiency and correction strategy. NMR Biomed 2011. doi: 10.1002/nbm.1675. [Epub ahead of print].
28. LaConte S, Strother S, Cherkassky V, Anderson J, Hu X. Support vector machines for temporal classification of block design fMRI data. Neuroimage 2005;26:317–329.
29. Hernandez-Garcia L, Lee GR, Vazquez AL, Noll DC. Fast, pseudo-continuous arterial spin labeling for functional imaging using a two-coil system. Magn Reson Med 2004;51:577–585.
30. Hernandez-Garcia L, Lee GR, Vazquez AL, Yip CY, Noll DC. Quantification of perfusion fMRI using a numerical model of arterial spin labeling that accounts for dynamic transit time effects. Magn Reson Med 2005;54:955–964.
31. Bagarinao E, Matsuo K, Nakai T, Sato S. Estimation of general linear model coefficients for real-time application. Neuroimage 2003;19:422–429.
32. Stone SS, Haldar JP, Tsao SC, Hwu WMW, Sutton BP, Liang ZP. Accelerating advanced MRI reconstructions on GPUs. J Parallel Distrib Comput 2008;68:1307–1318.
33. Gunther M, Oshio K, Feinberg DA. Single-shot 3D imaging techniques improve arterial spin labeling perfusion measurements. Magn Reson Med 2005;54:491–498.
34. Wang Z, Aguirre GK, Rao H, Wang J, Fern·ndez-Seara MA, Childress AR, Detre JA. Empirical optimization of ASL data analysis using an ASL data processing toolbox: ASLtbx. Magn Reson Imaging 2008;26:261–269.
35. Behzadi Y, Restom K, Liau J, Liu TT. A component based noise correction method (CompCor) for BOLD and perfusion based fMRI. Neuroimage 2007;37:90–101.